IEEE Access
Multidisciplinary | Rapid Review | Open Access Journal

Received 28 July 2024, accepted 13 August 2024, date of publication 19 August 2024, date of current version 28 August 2024.

Digital Object Identifier 10.1109/ACCESS.2024.3445877

APPLIED RESEARCH

An Imaging Algorithm for Multi-Channel SAR Azimuth Missing Data

WEI SONG AND YONGHONG YAO
School of Control Engineering, Wuxi Institute of Technology, Jiangsu, Wuxi 214121, China
Corresponding author: Wei Song (sw_818@163.com)

ABSTRACT In the process of synthetic aperture radar (SAR) data acquisition, aircraft are susceptible to various disturbances during flight, resulting in the loss or destruction of azimuth echo data, which leads to blurring of SAR images. To solve the problem of imaging blurring caused by missing data in azimuth, an imaging algorithm integrated with spectrum reconstruction based on adaptive beamforming is proposed. First, the multi-channel SAR azimuth missing data model is analyzed, and the multiple spatial freedoms provided by the multi-channel SAR system are applied to construct the spatial domain filter. Second, spatial adaptive beamforming is used for spatial filtering of each range-Doppler cell, and the spectrum of azimuth random missing data is reconstructed. Finally, the reconstructed spectrum data is imaged using the polar format algorithm (PFA). The point target simulation data and airborne multi-channel SAR real data are separately processed under the condition of both random and uniform missing data. Compared with the results of only PFA processing, the algorithm can eliminate false targets caused by periodic missing data and significantly improve the serious defocusing of point targets caused by random missing data. The entropy and the contrast of the real data image obtained by the proposed algorithm are improved by approximately 15% and 12%, respectively. The results verify the effectiveness of the algorithm.

INDEX TERMS Multi-channel SAR, azimuth missing data, adaptive beamforming, spectrum reconstruction.

I. INTRODUCTION

Synthetic aperture radar (SAR) is an active microwave detection sensor capable of obtaining high-resolution, two-dimensional images of the ground in all weather and all times [1]. It has been widely used in both military and civilian fields. Range pulse compression technology and azimuth synthetic aperture technology are used in SAR to achieve two-dimensional focusing imaging. The azimuth requires long coherent accumulation to create a virtual aperture; therefore, aircraft is susceptible to various disturbances during flight, which leads to the loss or destruction of azimuth echo data. Based on the type of lost data, it can be divided into periodic and random losses. The periodic loss of data mainly exists in specific situations, such as rotor occlusion echoes and specific working modes. The random loss of data is more common, often resulting from active interference with SAR radar, which can pollute and destroy the azimuth echo. Incompleteness of azimuth echo data leads to the defocusing of ground scene targets and seriously affects the imaging quality. Therefore, addressing the issue of missing SAR data in imaging is of great research value.

To address the problem of imaging ambiguity caused by the lack of SAR azimuth echo data, many scholars have begun to study and propose solutions. In [2], the interpolation method combined with linear prediction was used to complete the missing echo data, but the interpolation method required continuous data blocks, while the amount of missing data was small. In [3] and [4], Burg methods and the least-squares method were used to calculate the prediction coefficients, and then combined with the interpolation method to recover the missing data. These algorithms are sensitive to the prediction model and the signal-to-clutter ratio. When the missing signal is relatively large, the recovery of the missing data becomes exponentially attenuated, resulting in the radar image still exhibiting ghosting. Broersen

The associate editor coordinating the review of this manuscript and approving it for publication was Xuebo Zhang.

and Waeles [5] used the approximate maximum likelihood predictor with an autoregressive (AR) model to recover missing data. This type of algorithm, based on the AR model, is limited by model parameters. Owing to the lack of SAR echo data, it is usually difficult to determine the model parameters, resulting in poor quality of reconstructed imaging. In view of the shortcomings of parametric model methods, some scholars have proposed nonparametric adaptive filtering methods. These nonparametric algorithms mainly include the gapped data amplitude and phase estimation (GAPES) algorithm [6], [7] and the missing data iterative adaptive algorithm (MIAA) [8], [9]. These two algorithms are highly robust non-parametric missing data recovery methods based on spectral estimation. However, when they are applied to SAR, the problem of a large amount of data exists and cannot solve the problem of spectrum ambiguity. In [10], a method consists of phase compensation and recovering raw data in range doppler domain via generalised orthogonal matching pursuit to propose high-resolution SAR imaging from azimuth periodically gapped raw data. Jiang et al. [11] proposed a Sub-echo segmentation and reconstruction for azimuth missing data SAR imaging algorithm to solve the problem of incomplete echo SAR imaging. In [12], a method based on the Richardson–Lucy deconvolution algorithm is applied to spaceborne azimuth interrupted frequency modulation continuous wave SAR imaging to suppress ghost targets. In [13], a novel SAR imaging method for moving target with azimuth missing data, which can estimate and reconstruct the noncooperative moving target's complete echo from the azimuth incomplete echo based on its sparsity. These methods solve the problem of SAR imaging with missing azimuth data from different angles and all have unique advantages.

In recent years, some scholars have proposed the use of compressed sensing theory to reconstruct missing SAR echo data [14], [15], [16]. The compressed sensing theory of the sparse optimization method shows that, under the condition of for a sparse signal in a certain transform domain, the data obtained below the Nyquist sampling frequency can be reconstructed to recover the original signal. To address the problem of high computational complexity in compressed sensing SAR imaging algorithms, scholars have proposed a variety of improved algorithms. Fang et al. [17] proposed a sparse SAR imaging framework based on an approximate observational model. Yang et al. [18] proposed a two-dimensional sparse sampling algorithm that uses range-block processing to obtain a complete image. Duan et al. divided the original missing strip data into multiple sub-apertures, recovered each sub-aperture separately, and stitched them to obtain strip data [19]. Kang and Kim proposed a novel approach to compressed sensing SAR imaging based on improved Tikhonov regularization coupled with an adaptive strategy using iterative reweighted matrix to solve the compressed sensing reconstruction problem of SAR images with sparsity [20]. Kang and Baek presented an efficient compressive sensing based SAR imaging integrated with autofocus technique to improve the quality of imaging [21]. Bi et al. introduced sparse synthetic aperture radar imaging with $\ell 1$-norm regularization-based approximated observation method to recover the large-scale considered scene for down-sampled periodic data [22]. In [23], an incremental SAR imaging approach based on estimating the sensing dictionary matrix in the pursuit of sparsity is presented, which can address the issue that the irregular loss of received data and the nonuniformly under sampling yield the SAR azimuth ambiguity (SAA) resulting in the degradation in image quality. These improved algorithms for compressed sensing theory greatly reduce the amount of data calculation and improve computational efficiency.

Currently, the problem of recovering missing SAR echo data is primarily addressed in the single-channel dimension by using the algorithms mentioned above. Inspired by multichannel SAR digital beam-forming technology [24], [25], [26], this paper introduces the problem of missing SAR echo data recovery into multichannel SAR systems. Adaptive beam-forming methods can be used for spatial filtering on each range-Doppler cell, owing to the multiple spatial degrees of freedom provided by the multi-channel SAR system. The main lobe of spatial filtering is directed towards the direction corresponding to a spectral component while forming nulls in the directions of other spectral components, thereby isolating the Doppler spectrum component of that direction. After processing all the range-Doppler cells, the SAR echo spectrum can be reconstructed, enabling high-resolution imaging. To verify the effectiveness of the proposed method, point target simulations and actual data processing were performed for both periodic and random missing-data scenarios. The results show well-focused images, indicating that the algorithm proposed in this study can effectively address the problem of azimuth echo data loss in multichannel SAR.

The remainder of this paper is structured as follows. In Section II, a multi-channel SAR azimuth missing data model is established. Section III introduces the spectrum reconstruction algorithm based on adaptive beamforming, and the signal processing chain of the proposed imaging algorithm for multi-channel SAR azimuth missing data is presented. Based on the research in the previous sections, the processing results of the simulated data and real SAR radar data are discussed in Section IV. Finally, the paper is summarized and concluded in Section V.

II. MULTI-CHANNEL SAR AZIMUTH MISSING DATA MODEL

In an airborne multichannel SAR system, multiple receiving channels are arranged along a track. The full aperture is used to transmit signals, and all the receiving channels receive echo signals simultaneously. In this study, it is assumed that the multichannel SAR antenna array is a uniform linear array, with N receiving channels and a carrier aircraft speed of v. The transmitted signal of a multichannel SAR system can be

expressed as defined by Equation (1).

$$s(\tau) = \text{rect}\left(\frac{\tau}{T_r}\right) \cdot \cos\left(2\pi f_0 \tau + \pi K_r \tau^2\right) \tag{1}$$

where f_0 is the center frequency of the transmitted signal, K_r is the frequency modulation slope of the transmitted signal, τ is the distance dimension time, T_r is the pulse repetition period, and rect$(\cdot)$ represents a rectangular function as defined in Equation (2).

$$\text{rect}(\text{x}) = \begin{cases} 1, & |\text{x}| \le 0.5 \\ 0, & \text{else} \end{cases} \tag{2}$$

Because multiple receiving antennas are arranged in a linear array, the echo signals from each receiving channel exhibit a fixed time-delay phase difference. The range-Doppler domain expression of the received echo signal for the mth channel is given by Equation (3).

$$s_m(\tau, f_d) = s_0(\tau, f_d) \cdot \exp\left(\frac{j2\pi x_m}{v} f_d\right) \tag{3}$$

where $s_0(\tau, f_d)$ is the echo signal received by the first receiving channel, x_m is the distance between the mth receiving channel and the first receiving channel, and f_d is the Doppler frequency of the target, which can be expressed as show in Equation (4).

$$f_d = \frac{2\text{v}\sin\varphi \cdot \sin\theta}{\lambda} \tag{4}$$

where λ is the wavelength of the radar-transmitting pulse, φ is the elevation angle of the radar beam pointing, and θ is the azimuth angle of the radar beam pointing. Therefore, there is a linear relationship between the Doppler frequency and the sine value of the azimuth angle of the beam pointing.

When there is missing data in the azimuth direction, the echo signal is modulated by multiple spectra in the azimuth frequency domain, resulting in the echo signal of each range-Doppler unit being superimposed by the echo signals from multiple range-Doppler units with different azimuths. The echo signal of the nth receiving channel can be expressed using Equation (5).

$$s_n^k(\tau, f_d) = \sum_{k=0}^{k-1} s(\tau, f_d + f_k) \cdot \exp\left(\frac{j2\pi x_n}{v}(f_d + f_k)\right) \tag{5}$$

where k is the number of times the spectrum is modulated and f_k is the kth modulated spectrum component.

Let the column vector $\mathbf{a}_k(f_d)$ represent the spatial steering vector corresponding to the kth modulated spectral component. Then, the column vector $\mathbf{a}_k(f_d)$ can be expressed as show in Equation (6):

$$\mathbf{a}_k(f_d) = \left[e^{\frac{j2\pi d}{v}(f_d+f_k)}, \cdots, e^{\frac{j2\pi nd}{v}(f_d+f_k)}, \cdots, e^{\frac{j2\pi Nd}{v}(f_d+f_k)}\right]^T \tag{6}$$

where superscript T represents the rank operation and d is the distance between two adjacent channels. The received data vector of the array can then be expressed in Equation (7).

$$\mathbf{x}(\tau, f_d) = \mathbf{A}(f_d)\,\mathbf{p}(\tau, f_d)\,\mathbf{A}(f_d) + \mathbf{e}(\tau, f_d) \tag{7}$$

where $\mathbf{e}(\tau, f_d)$ denotes the white noise component of each receiving channel, and the expressions for $\mathbf{A}(f_d)$ and $\mathbf{p}(\tau, f_d)$ are shown in Equation(8) and Equation(9), respectively.

$$\mathbf{A}(f_d) = [a_0(f_d), a_1(f_d), \cdots, a_{k-1}(f_d)] \tag{8}$$

$$\mathbf{p}(\tau, f_d) = [p(\tau, f_d), p(\tau, f_d + f_1), \cdots, p(\tau, f_d + f_{k-1})]^T \tag{9}$$

III. SPECTRUM RECONSTRUCTION ALGORITHM AND IMAGING ALGORITHM FLOW

A. SPECTRUM RECONSTRUCTION ALGORITHM PRINCIPLE

According to the signal model of the multi-channel SAR azimuth missing data introduced in the previous section, spectrum reconstruction can be achieved by adaptive beamforming technology using multiple degrees of freedom provided by the multichannel SAR system. In the range-Doppler unit, to extract the Doppler spectrum component in a certain direction, the main beam of the array response points in the direction corresponding to the spectrum component, and beam nulls are formed in the directions of the other spectrum component. Then, the Doppler spectrum frequency in all directions can be reconstructed by processing the range-Doppler units one by one. In spatial adaptive beamforming [27], the minimum variance distortionless response (MVDR) beamformer proposed by Capon [28] is a typical representative of beamforming algorithms that can be used to solve the problem of spectrum reconstruction of multichannel SAR data. The array weight vector of the Capon beamformer is obtained using Equation (10).

$$\begin{cases} \min \mathbf{w}(f_d + f_k)^H \mathbf{R}(f_d + f_k)\,\mathbf{w}(f_d + f_k) \\ subject \mathbf{w}(f_d + f_k)^H \mathbf{a}_k(f_d) = 1 \end{cases} \tag{10}$$

where the superscript H represents the conjugate rank operation, and $\mathbf{R}(\tau, f_d)$ is the autocorrelation matrix of the received echo data, as shown in Equation (11).

$$\mathbf{R}(\tau, f_d) = \mathbf{x}(\tau, f_d)\,\mathbf{x}(\tau, f_d)^H \tag{11}$$

Combining equation (10) and equation (11), we can obtain the weight vector, as shown in Equation (12):

$$\mathbf{w}(f_d + f_k) = \frac{\mathbf{R}^{-1}(\tau, f_d)\,\mathbf{a}_k(f_d)}{\mathbf{a}_k^H(f_d)\,\mathbf{R}^{-1}(\tau, f_d)\,\mathbf{a}_k(f_d)} \tag{12}$$

The extraction of the kth Doppler spectrum component is expressed by Equation (13).

$$\hat{p}(\tau, f_d + f_k) = \mathbf{w}(f_d + f_k)^H \mathbf{x}(\tau, f_d) \tag{13}$$

The spectrum of multichannel SAR data can be reconstructed after processing all range-Doppler units according to Equation (13).

B. IMAGING ALGORITHM FLOW FOR MULTI-CHANNEL SAR AZIMUTH MISSING DATA

In this study, spatial adaptive beamforming technology was used to reconstruct the azimuth spectrum, and the spectrum reconstruction was integrated into the Polar Format Algorithm (PFA) imaging [29], [30]. The flowchart of the algorithm is shown in Figure 1.

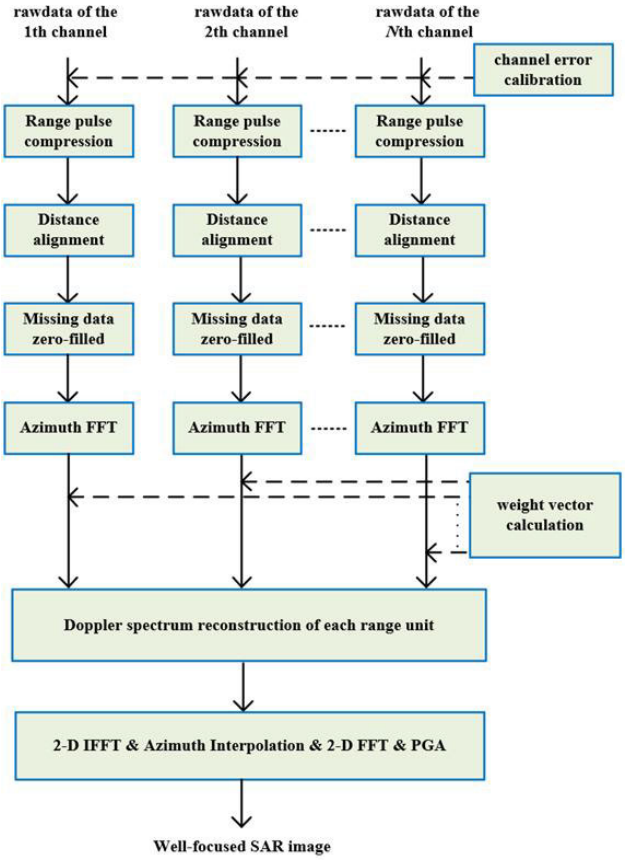

FIGURE 1. Flowchart of imaging algorithm for azimuth missing data.

The detailed steps are as follows:

1) Process the original echo data in the distance dimension, which includes channel error calibration, pulse compression, and range alignment (interpolation and phase compensation).
2) Set the missing or destroyed azimuth echo data to zero.
3) Azimuth FFT is performed on the echo data of each channel obtained by preprocessing to obtain the range Doppler domain image data expressed as (3).
4) The optimal weight vector of the MVDR beamformer is calculated according to (8). Each Doppler component is calculated according to (9), and then combined to obtain the complete Doppler spectrum. The adaptive reconstruction of the Doppler spectrum is performed for each range unit.
5) A two-dimensional Fourier inverse transform is applied to the resulting data of the fourth step, and then interpolation processing is performed in the azimuth. The coarse-focused image is obtained a two-dimensional Fourier transform. Finally, the well-focused SAR image can be obtained by the phase gradient autofocus (PGA) processing.

IV. SIMULATION AND REAL DATA PROCESSING

In this section, the effectiveness of the proposed algorithm is verified by processing point-target simulation echo data and multi-channel airborne SAR actual echo data. The robustness of the spectrum reconstruction algorithm based on adaptive beamforming was tested for two cases of azimuth periodic missing data and random missing data.

A. SIMULATION RESULTS

First, we focused on processing the simulated data. The SAR parameters are listed in Table 1. In the simulation experiment, it was assumed that there were three point targets in the radar observation scene and had the same radar cross-sectional area. The 2-D SAR original echo data of 4096×4096 pixels were obtained without adding noise. We modified the echo data to periodically missing and randomly missing by setting the pulse echo to zero periodically and randomly, respectively.

TABLE 1. Parameters of the multi-channel SAR.

Parameter	Value	Units
signal wavelength	0.3	cm
signal bandwidth	500	MHz
sampling rate	600	MHz
pulse width	6	us
pulse repetition frequency	1600	Hz
airplane speed	120	m/s
transmitter antenna aperture	0.5	m
receiver antenna aperture	0.5	m
receiver antenna array length	1.5	m

1) PERIODIC MISSING DATA IMAGING RESULTS

In the simulation experiment of periodic missing data, we extracted one pulse every three pulses and set 1365 azimuth pulses to zero. For this periodic missing data, the azimuth spectrum in the range-Doppler domain is shown in Figure 2, where the dotted line represents the azimuth spectrum of the periodic missing data, and the solid line is the azimuth spectra of the complete data. It can be seen that the azimuthal periodic missing data cause the azimuth spectrum to be modulated, and two spectra are superimposed on the original spectrum. The imaging results for the azimuthal periodic missing data are shown in Figure 3. Figure 3(a) shows the image processed only by PFA, from which it can be seen that each point target is modulated with two false targets, and the false targets defocuses seriously. Figure 3(b) shows the image processed by the proposed algorithm in which the false targets are eliminated.

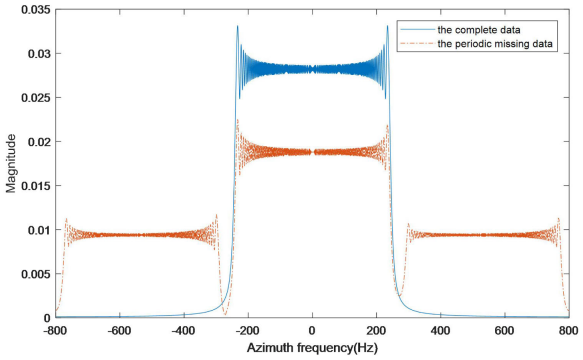

FIGURE 2. Azimuth spectrum of azimuth periodic missing data and complete data.

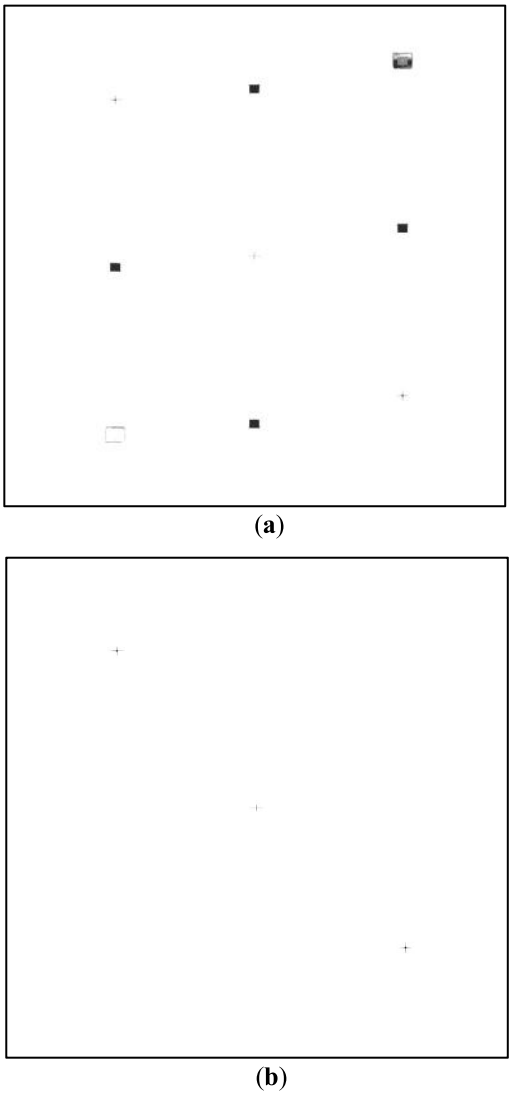

FIGURE 3. Imaging results of periodic missing data by using different algorithms. (a) Only PFA imaging result. (b) Imaging result of the proposed algorithm.

2) RANDOM MISSING DATA IMAGING RESULTS

We randomly set 1365 azimuth pulses in the original echo data to zero according to a uniform distribution. For this random missing data, the azimuth spectrum in the range-Doppler domain is shown in Figure 4, where the dotted line represents the azimuth spectrum of the random missing data, and the solid line is the azimuth spectrum of the complete data. We can see that the azimuth spectrum of random missing data is superimposed with multiple modulated spectra, and it becomes disorganized. The imaging results of the azimuthal random missing data are shown in Figure 5. Figure 5(a) shows the image processed using only PFA imaging and autofocus, from which it can be seen that each point target is seriously defocused in the azimuth direction. Figure 5(b) shows the image processed by the proposed algorithm, in which the point targets are well-focused.

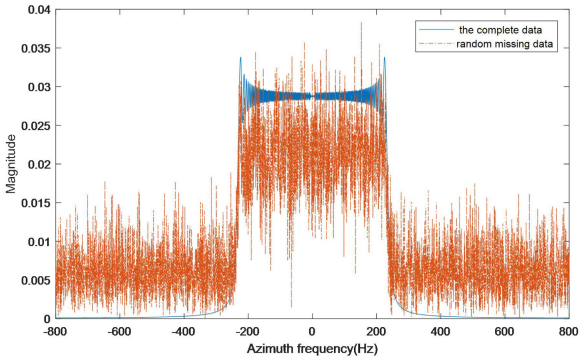

FIGURE 4. Azimuth spectrum of azimuth random missing data.

B. REAL DATA PROCESSING RESULTS

In this section, the algorithm of this study is further verified by processing the experimental data from the actual flight of an airborne multichannel SAR. The main parameters of the radar are as follows. The bandwidth of the transmitted linear frequency modulation signal is 180MHz. Wavelength is the 0.3 cm, the pulse repetition frequency is 1250 Hz, and the sampling rate is 200 MHz. Similar to the simulation experiment, the original echo data were modified to periodic missing and random missing, and a total of 1365 azimuth pulses were set to zero. For convenience of display, a part of the azimuth echo at the scene center distance unit is shown in Figure 6.

1) PERIODIC MISSING DATA IMAGING RESULTS

The imaging results for the periodic missing data are shown in Figure 7. Figure 7(a) shows the results of using only PFA imaging and autofocus, where the scene is blurred. Figure 7(b) shows the result of periodic missing data processing using the algorithm proposed in this paper, where the image is clear and the target is well-focused. The isolated strong target in the red box of Figure 7 was selected to analyze the focusing performance of the strong point target. The results are shown in Figure 8. we can see that compared with the imaging results without doppler spectrum reconstruction, after the doppler spectrum reconstruction algorithm processing, the amplitude value of the point target increased from

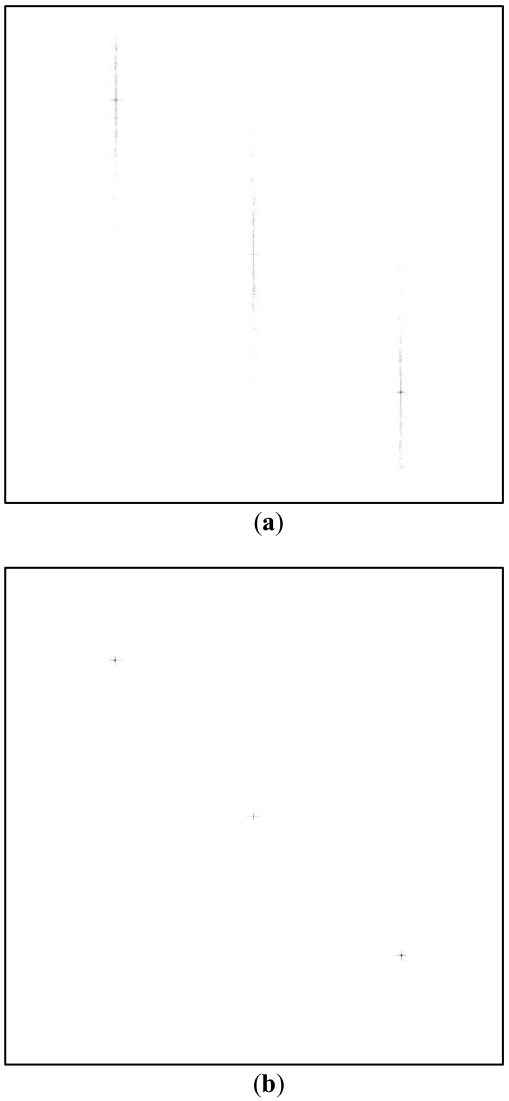

FIGURE 5. Imaging results of random missing data by using different algorithms. (a) Only PFA imaging result. (b) Imaging result of the proposed algorithm.

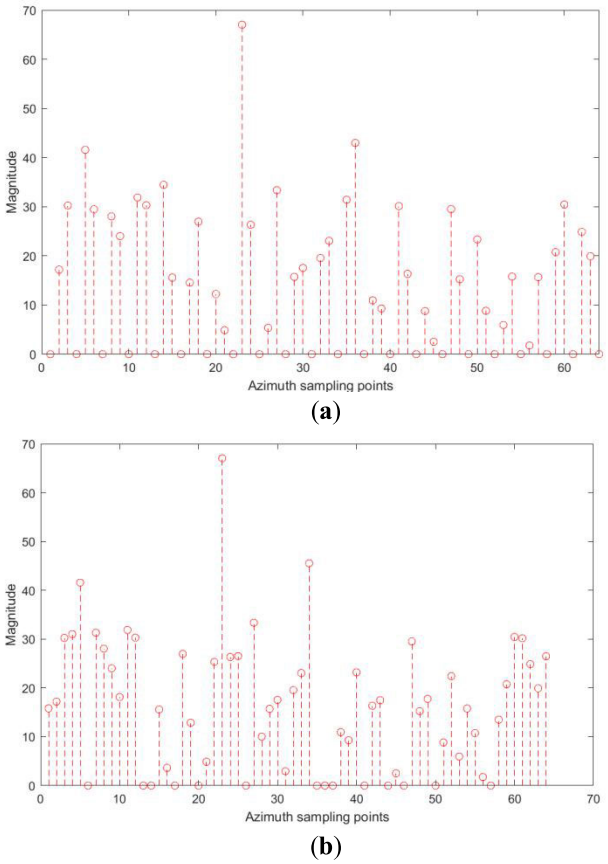

FIGURE 6. Part of the azimuth echo of missing 1365 azimuth pulses. (a) Part of the azimuth echo with periodic missing data. (b) Part of the azimuth echo with random missing data.

about 7 to 15, which proves that the image has a higher signal-to-noise ratio and that focusing effect is greatly improved.

2) RANDOM MISSING DATA IMAGING RESULTS

The imaging results for the random missing data are shown in Figure 9. Figure 9(a) shows the results of PFA imaging and autofocus, and we can see that the target in the image is seriously defocused. Figure 9(b) shows the results of random missing data processing using the proposed algorithm, where the scene is well-focused. The azimuth slice of the strong-point target in Figure 9 (the same target at the red frame position in Figure 7) is shown in Figure 10.

It can be seen that the amplitude of the isolated strong-point target is approximately 4 in the results without Doppler spectrum reconstruction, which is almost equal to the amplitude of other weak reflection scattering points around it. In the results processed by the algorithm in this study, the amplitude value of the isolated strong-point target is approximately 15, which is significantly higher than that of the other scattering points around. The comparison of the two slices proves that the proposed method can improve the imaging and focusing effect of random missing data.

3) THE INFLUENCE OF THE NUMBERS OF MISSING DATA ON THE IMAGING RESULTS

To further evaluate the performance of the proposed algorithm and measure the effect of missing azimuth pulses on the processing results, we randomly set 2730 azimuth pulses to zero in the original SAR echo data. The SAR images obtained using the proposed algorithm are shown in Figure 11. It can be observed from the figure that the entire image remains clear, but the overall brightness decreases.

The azimuth slices of the isolated strong-point target in the imaging results of with 1365 missing pulses and 2730 missing pulses are shown, as shown in Figure 12.

From the azimuth slices shown in Figure 12, we can see that the targets are all well focused in both cases of random loss of 1365 and 2730 pulses in the azimuth. However, the higher the number of lost pulses, the lower is the

TABLE 2. SAR image quality comparison of different algorithms.

Types of missing data	Entropy			Contrast		
	PFA	Proposed algorithm	Improvement ratio	PFA	Proposed algorithm	Improvement ratio
Periodic missing	44.8	38.0	15.0%	0.57	0.64	12.2%
Random missing	43.5	37.2	14.5%	0.58	0.63	8.6%

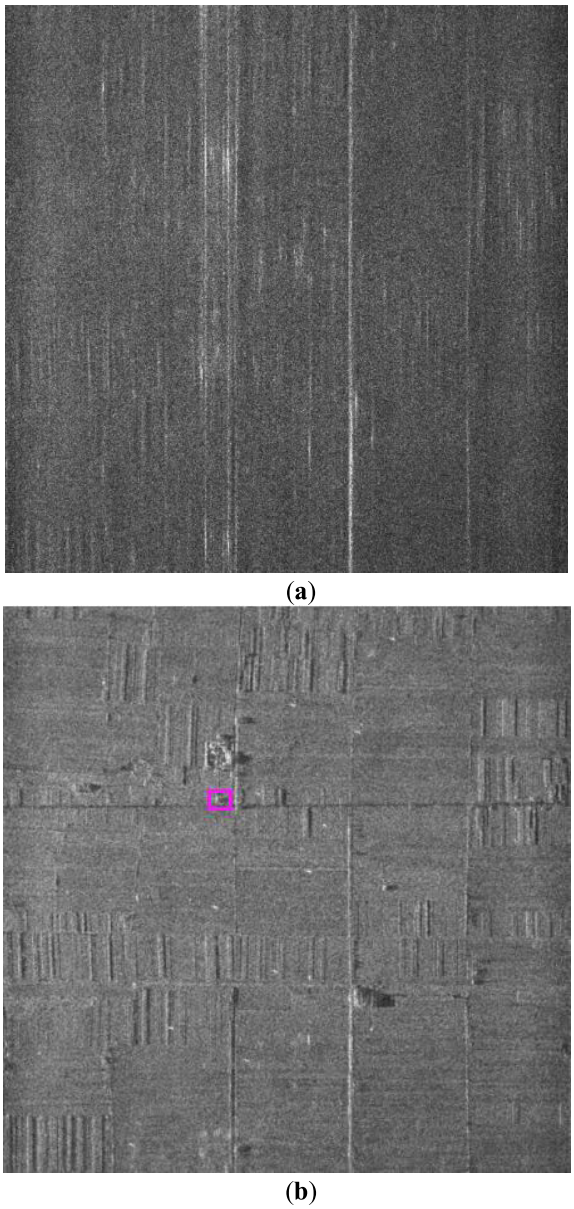

FIGURE 7. Imaging results of actual periodic missing data by using different algorithms. (a) Only PFA imaging result. (b) Imaging result of the proposed algorithm.

signal-to-noise ratio of the target, which is also true in theory. Therefore, in terms of image focusing performance, the proposed algorithm is insensitive to the number of azimuth pulse losses and has strong robustness.

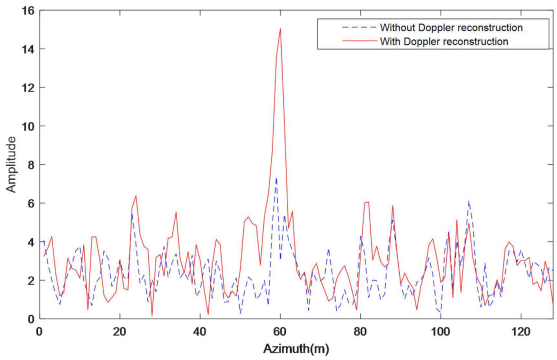

FIGURE 8. Azimuth slice of periodic missing data image.

C. QUANTITATIVE COMPARISON OF IMAGE QUALITY

To quantitatively evaluate the performance of the proposed algorithm, we assessed the image-focusing quality based on the entropy and contrast of the image. The calculation equation for the entropy of a two-dimensional SAR image is shown in Equation (14).

$$E(I) = -\sum_{q=0}^{Na-1}\sum_{k=0}^{Nr-1} D(q,k)\ln D(q,k) \tag{14}$$

Here, Na represents the total number of azimuth pulses in the SAR image, and Nr denotes the number of range cells in the SAR image. $D(q,k)$ is the scattering intensity density of the image, as shown in Equation (14), where $I(q,k)$ is the intensity of each pixel of the SAR image.

$$D(q,k) = \frac{[I(q,k)]^2}{\sum_{q=0}^{Na-1}\sum_{k=0}^{Nr-1} I(q,k)} \tag{15}$$

It can be seen from Equations (14) and (15) that the clearer the SAR image, the smaller the entropy value. The contrast of an image is also an important indicator for measuring its clarity. The contrast value of the well-focused SAR image is relatively high, and the contrast value of the fully focused SAR image reaches its maximum. The image contrast expression is defined by Equation (16).

$$C = \frac{\sqrt{\mathrm{E}\left\{[I(q,k)]^2 - \mathrm{E}\left\{[I(q,k)]^2\right\}\right\}}}{\mathrm{E}\left\{[I(q,k)]^2\right\}} \tag{16}$$

where $E(\cdot)$ is the expectation operator.

The entropy and contrast of the four images in Figure 7 and Figure 9 were calculated and are shown in Table 2. It can be seen intuitively from the data in the table that compared with

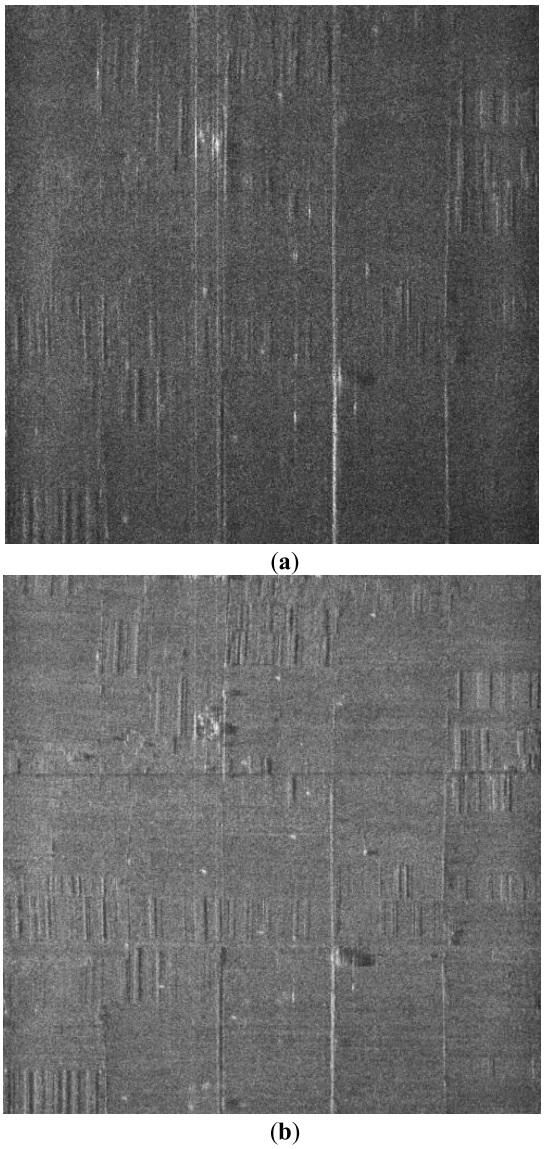

FIGURE 9. Imaging results of actual random missing data by using different algorithms. (a) Only PFA imaging result. (b) Imaging result of the proposed algorithm.

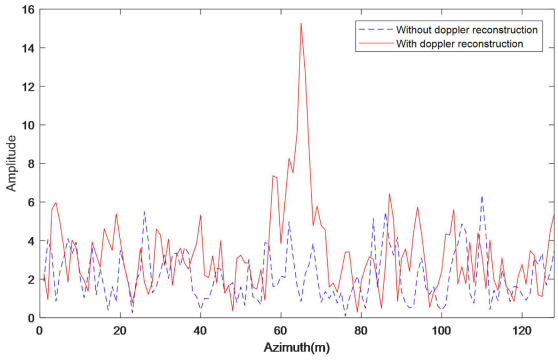

FIGURE 10. Azimuth slice of random missing data image.

only PFA processing, the entropy of the image obtained by the proposed algorithm for periodically missing data and random

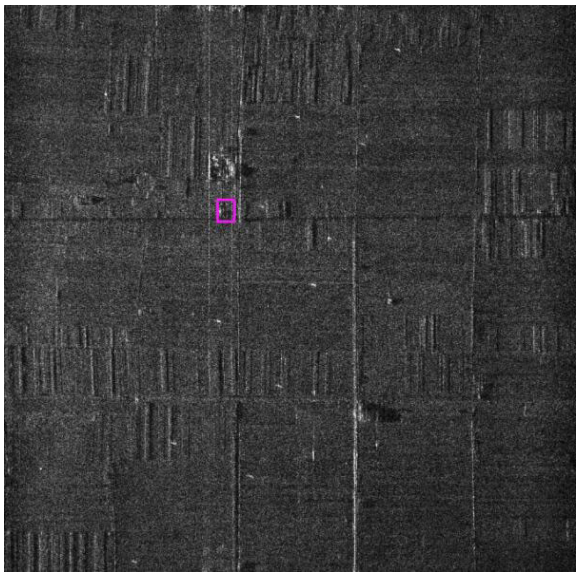

FIGURE 11. Imaging results for actual data with random missing 2730 pulses in azimuth.

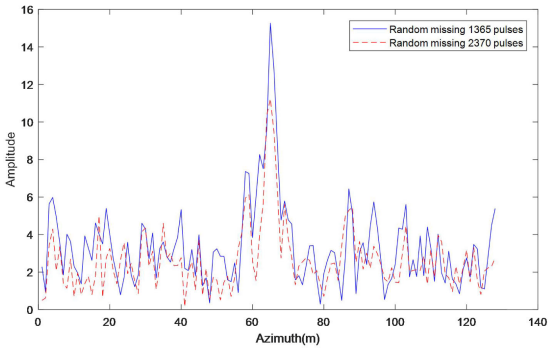

FIGURE 12. Azimuth slice of strong point target with missing different number of azimuth pulses.

missing data are reduced from 44.8 to 38.0, from 43.5 to 37.2, the improvement ratio is approximately 15 %. It can also be seen that the contrast of the image obtained by the proposed algorithm for periodically missing data and random missing data are respectively increased from 0.57 to 0.64, from 0.58 to 0.63, the improvement ratio are respectively12.2%, 8.6%. The improvement in the two image quality parameters further indicates that the proposed algorithm can effectively improve the focusing quality of SAR images.

D. ALGORITHM COMPLEXITY ANALYSI

The proposed algorithm recovers the damaged azimuth spectrum through spectrum reconstruction, which is then integrated into PFA imaging. Therefore, compared with the PFA algorithm, the increased computational complexity is mainly due to spectrum reconstruction. We use complex multiplication to measure the computational complexity of the spectrum reconstruction algorithm. In the spectrum reconstruction, the sample covariance matrix such as show in

Formula (11) is first calculated, and the amount of computation is as shown in Equation (17).

$$f_1 = N_r N^2 \tag{17}$$

where Nr is the number of range cells in the SAR, and N denotes the number of SAR receiving channels.

The inverse operation of the covariance matrix can decompose the floating-point operations into finer basic multiplication operation, and the calculation amount is shown in Equation (18).

$$f_2 = N^3 \tag{18}$$

The computational amount of the weight vector shown in Equation (12) and the beamforming shown in Equation (13) is expressed in Equation (19).

$$f_3 = 4N + N_r N \tag{19}$$

Then the total computational amount can be expressed in Equation (20)

$$\begin{aligned} f &= N_a \left(f_1 + f_2 + f_3\right) \\ &= N_a \left(N_r N^2 + N^3 + 4N + N_r N\right) \end{aligned} \tag{20}$$

where Na is the total number of azimuth pulses of the SAR image.

It can be seen from Equation (19) that the increased computational complexity is proportional to the number of azimuth pulses, the number of range points and the number of channels. The increased amount of calculation will increase exponentially with the increase in the number of channels. Therefore, we need to make a compromise between the number of channels and the performance of the algorithm. Parallel processing can be used to improve the computational efficiency, which is not discussed in this paper further.

V. CONCLUSION

In this study, we attempt to find a solution in the multichannel SAR system to address the problem of imaging blurring caused by missing azimuth data. A novel azimuth spectrum reconstruction algorithm based on spatial domain adaptive beamforming technology is proposed. The main beam of the spatial domain filter points in the direction corresponding to a certain spectral component, whereas beam zeros are formed in the direction of other spectral components. After azimuth spectrum filtering of the multichannel data, the Doppler spectrum component corresponding to the main beam direction can be obtained. After processing all range-Doppler cells, complete and orderly spectra can be reconstructed. This azimuth spectrum reconstruction is then integrated into a polar-format imaging algorithm. The processing results of the point target simulation data and actual multi-channel SAR airborne echo data demonstrate that the proposed algorithm can reconstruct the azimuth spectrum in both periodic and random missing data scenarios, which improves the clarity of SAR images. The experimental results also demonstrated that the algorithm was robust.

The limitations of the algorithm in this study is that, first, in the operation of azimuth spectrum reconstruction, the amplitude and phase responses of each channel of the radar must be consistent [31], [32]. However, in practical engineering applications, errors exist, such as in antenna installation and position measurement. These errors inevitably reduce the performance of the algorithm. Therefore, it is necessary to further study multichannel amplitude and phase-error correction technology. Additionally, the algorithm proposed in this study requires matrix inversion and other operations. It is necessary to further optimize the algorithm to improve its real-time performance.

REFERENCES

[1] W. M. Brown, "Synthetic aperture radar," *IEEE Trans. Aerospace Electron. Syst.*, vol. AES-3, pp. 217–229, Mar. 1967.
[2] I. J. Gupta, "High-resolution radar imaging using 2-D linear prediction," *IEEE Trans. Antennas Propag.*, vol. 42, no. 1, pp. 31–37, Jan. 1994.
[3] I. J. Gupta, M. J. Beals, and A. Moghaddar, "Data extrapolation for high resolution radar imaging," *IEEE Trans. Antennas Propag.*, vol. 42, no. 11, pp. 1540–1545, Nov. 1994.
[4] I. Erer, "A new data extrapolation algorithm for high resolution ISAR imaging," *AEU Int. J. Electron. Commun.*, vol. 60, no. 4, pp. 316–319, Apr. 2006.
[5] P. M. T. Broersen, S. de Waele, and R. Bos, "Estimation of autoregressive spectra with randomly missing data," in *Proc. 20th IEEE Instrum. Technol. Conf.*, vol. 2, Vail, CO, USA, May 2003, pp. 1154–1159.
[6] P. Stoica, E. G. Larsson, and J. Li, "Adaptive filter-bank approach to restoration and spectral analysis of gapped data," *Astronomical J.*, vol. 120, no. 4, pp. 2163–2173, Oct. 2000.
[7] E. G. Larsson, P. Stoica, and J. Li, "Amplitude spectrum estimation for two-dimensional gapped data," *IEEE Trans. Signal Process.*, vol. 50, no. 6, pp. 1343–1354, Jun. 2002.
[8] T. Yardibi, J. Li, P. Stoica, M. Xue, and A. B. Baggeroer, "Source localization and sensing: A nonparametric iterative adaptive approach based on weighted least squares," *IEEE Trans. Aerosp. Electron. Syst.*, vol. 46, no. 1, pp. 425–443, Jan. 2010.
[9] D. Vu, L. Xu, M. Xue, and J. Li, "Nonparametric missing sample spectral analysis and its applications to interrupted SAR," *IEEE J. Sel. Topics Signal Process.*, vol. 6, no. 1, pp. 1–14, Feb. 2012.
[10] Y. Qian and D. Zhu, "High-resolution SAR imaging from azimuth periodically gapped raw data via generalised orthogonal matching pursuit," *Electron. Lett.*, vol. 54, no. 21, pp. 1235–1237, Oct. 2018.
[11] N. Jiang, J. Zhu, D. Feng, Z. Xie, J. Wang, and X. Huang, "High-resolution SAR imaging with azimuth missing data based on sub-echo segmentation and reconstruction," *Remote Sens.*, vol. 15, no. 9, p. 2428, May 2023.
[12] K. Liu, W. Yu, J. Lv, and Z. Tang, "Parameter design and imaging method of spaceborne azimuth interrupted FMCW SAR," *IEEE Geosci. Remote Sens. Lett.*, vol. 19, pp. 1–5, 2022.
[13] N. Jiang, J. Wang, D. Feng, N. Kang, and X. Huang, "SAR imaging method for moving target with azimuth missing data," *IEEE J. Sel. Topics Appl. Earth Observ. Remote Sens.*, vol. 15, pp. 7100–7113, 2022.
[14] L. C. Potter, E. Ertin, J. T. Parker, and M. Cetin, "Sparsity and compressed sensing in radar imaging," *Proc. IEEE*, vol. 98, no. 6, pp. 1006–1020, Jun. 2010.
[15] J. H. G. Ender, "On compressive sensing applied to radar," *Signal Process.*, vol. 90, no. 5, pp. 1402–1414, May 2010.
[16] S.-J. Wei, X.-L. Zhang, J. Shi, and G. Xiang, "Sparse reconstruction for SAR imaging based on compressed sensing," *Prog. Electromagn. Res.*, vol. 109, pp. 63–81, 2010.
[17] J. Fang, Z. Xu, B. Zhang, W. Hong, and Y. Wu, "Fast compressed sensing SAR imaging based on approximated observation," *IEEE J. Sel. Topics Appl. Earth Observ. Remote Sens.*, vol. 7, no. 1, pp. 352–363, Jan. 2014.
[18] J. Yang, J. Thompson, X. Huang, T. Jin, and Z. Zhou, "Segmented reconstruction for compressed sensing SAR imaging," *IEEE Trans. Geosci. Remote Sens.*, vol. 51, no. 7, pp. 4214–4225, Jul. 2013.
[19] H. Duan, D. Zhu, R. Li, and D. Wu, "Recovery and imaging method for missing data of the strip-map SAR based on compressive sensing," *Syst. Eng. Electron.*, vol. 38, no. 5, pp. 1025–1031, 2016.

[20] M.-S. Kang and K.-T. Kim, "Compressive sensing based SAR imaging and autofocus using improved Tikhonov regularization," *IEEE Sensors J.*, vol. 19, no. 14, pp. 5529–5540, Jul. 2019, doi: 10.1109/JSEN.2019.2904611.
[21] M.-S. Kang and J.-M. Baek, "Efficient SAR imaging integrated with autofocus via compressive sensing," *IEEE Geosci. Remote Sens. Lett.*, vol. 19, pp. 1–5, 2022, doi: 10.1109/LGRS.2022.3213251.
[22] H. Bi, X. Lu, Y. Yin, W. Yang, and D. Zhu, "Sparse SAR imaging based on periodic block sampling data," *IEEE Trans. Geosci. Remote Sens.*, vol. 60, 2022, Art. no. 5213812, doi: 10.1109/TGRS.2021.3110772.
[23] M.-S. Kang and J.-M. Baek, "SAR image reconstruction via incremental imaging with compressive sensing," *IEEE Trans. Aerosp. Electron. Syst.*, vol. 59, no. 4, pp. 4450–4463, Aug. 2023, doi: 10.1109/TAES.2023.3241893.
[24] W. Wang, R. Wang, Y. Deng, W. Xu, L. Guo, and L. Hou, "Azimuth ambiguity suppression with an improved reconstruction method based on antenna pattern for multichannel synthetic aperture radar systems," *IET Radar, Sonar Navigat.*, vol. 9, no. 5, pp. 492–500, Jun. 2015.
[25] F. Bordoni, M. Younis, and G. Krieger, "Ambiguity suppression by azimuth phase coding in multichannel SAR systems," *IEEE Trans. Geosci. Remote Sens.*, vol. 50, no. 2, pp. 617–629, Feb. 2012.
[26] M. Shen, L. Yang, D. Wu, and D. Zhu, "Multichannel SAR wide-swath imaging based on adaptive removal of azimuth ambiguities," *Remote Sens. Lett.*, vol. 6, no. 8, pp. 628–636, Aug. 2015.
[27] W. L. Melvin, "A STAP overview," *IEEE Aerosp. Electron. Syst. Mag.*, vol. 19, no. 1, pp. 19–35, Jan. 2004.
[28] M. Rubsamen and M. Pesavento, "Maximally robust capon beamformer," *IEEE Trans. Signal Process.*, vol. 61, no. 8, pp. 2030–2041, Apr. 2013.
[29] A. W. Doerry, "Wavefront curvature limitations and compensation to polar format processing for synthetic aperture radar images," Sandia Nat. Laboratories, Albuquerque, NM, USA, Sandia Tech. Rep. SAND2007-0046, 2007.
[30] L. Ding, X. Mao, and D. Zhu, "Polar format algorithm wavefront curvature error compensation using 2D space-variant post-filtering," *Acta Aeronautica et Astronautica Sinica*, vol. 36, pp. 605–613, Feb. 2015.
[31] A. Albaba, M. Bauduin, T. Verbelen, H. Sahli, and A. Bourdoux, "Forward-looking MIMO-SAR for enhanced radar imaging in autonomous mobile robots," *IEEE Access*, vol. 11, pp. 66934–66948, 2023, doi: 10.1109/ACCESS.2023.3291611.
[32] J. W. Smith and M. Torlak, "Efficient 3-D near-field MIMO-SAR imaging for irregular scanning geometries," *IEEE Access*, vol. 10, pp. 10283–10294, 2022, doi: 10.1109/ACCESS.2022.3145370.

WEI SONG was born in Pizhou, China, in 1980. He received the Ph.D. degree in communication and information systems from Nanjing University of Aeronautics and Astronautics, Nanjing, in 2015. From August 2005 to March 2022, he was a Radar Algorithm Designer with the Leihua Electronic Technology Research Institute, China Aviation Industry. He has been a Senior Engineer of radar science and technology, since 2012. Since April 2022, he has been an Associate Professor with the School of Control Engineering, Wuxi Institute of Technology, China. He was the author of more than ten articles. His research interests include SAR imaging algorithms and SAR system designs.

YONGHONG YAO was born in Shaoyang, China, in 1984. He received the M.S. degree in signal and information processing from Harbin Engineering University, Harbin, in 2011. From April 2011 to March 2021, he was a Radar Algorithm Designer with the Leihua Electronic Technology Research Institute, China Aviation Industry. He has been a Senior Engineer of radar science and technology, since 2019. Since April 2021, he has been an Associate Professor with the School of Control Engineering, Wuxi Institute of Technology, China. He was the author of more than ten articles. His research interests include SAR imaging algorithms and SAR system designs.